a = radius of perfectly conducting circular cylinder
a' = semimajor axis of an ellipse
b = radial distance to location of antenna in circular cylindrical co-ordinates
b' = semiminor axis of an ellipse
c_n = series coefficient (see (51))
c_n' = series coefficient (see (60))
d = half the distance between foci of the ellipses
d_n = series coefficient (see (52))
d_n' = series coefficient (see (61))
h_1 = metrical coefficient $h_1 = d\sqrt{\cosh^2 u - \cos^2 v}$
k = propagation constant, $k = 2\pi/\lambda$
l = effective length of dipole or loop antenna
r = radial distance from origin
$s = k^2 d^2 \sin^2\theta_0$
u = radial co-ordinate in elliptic cylinder co-ordinates
u_0 = radial co-ordinate for surface of perfectly conducting elliptical cylinder
u_1 = radial co-ordinate of location of antenna
v = angular co-ordinate in elliptic cylinder co-ordinates
v_1 = angular co-ordinate of location of antenna
$w = kb \sin\theta_0$ (see Table II)
z = axial co-ordinate
Π = Hertzian vector potential
Π^* = Hertzian vector potential
γ = separation constant, $\gamma = k \cos\theta_0$
ϵ = dielectric constant of free space, $\epsilon = 10^{-9}/36\pi$
ϵ_n = Neumann's number ($\epsilon_0 = 1$; $\epsilon_n = 2$ if $n \neq 0$)
θ_0 = angle between z axis and direction of propagation
λ = wavelength in free space
μ = permeability of free space, $\mu = 4\pi \times 10^{-7}$
$\xi = \xi_1 = \cosh u_1$ (see Table I)
ρ = radial co-ordinate in circular cylindrical co-ordinates
ϕ = azimuthal angular co-ordinate
ϕ_0 = azimuthal angle of direction of propagation.

Current Distributions on Helical Antennas*

JAMES A. MARSH†, ASSOCIATE, IRE

Summary—**The current distribution on a uniform circular helix has been measured over a frequency band extending from 600 to 1,700 mc. Although the measured distributions are highly complex functions of distance and also change in an anomalous manner with frequency, it is possible to analyze the distributions in terms of traveling waves associated with three different transmission modes on the helix. The relative amplitude functions of these traveling waves, as well as their associated phase velocities, are approximated. Current distributions which have been calculated by superposing three or more traveling waves are in good agreement with the measured data.**

I. Introduction

IN RECENT years considerable effort has been spent in analyzing the propagation of electrical energy along a helical conductor. Many applications of the helix have been found. One of these, discovered by Kraus,[1-5] employs the helix as an end-fire antenna. In this application the pitch angle may lie between 10 and 20 degrees while the circumference of the imaginary cylinder having diameter D (see Fig. 1) is approximately 0.80 to 1.3 wavelengths. In this range of frequencies a helix, of at least a few turns, radiates approximately circularly polarized waves in the direction of its axis. The radiation pattern of this antenna has a beamwidth which may be made quite narrow by employing a sufficiently large number of turns. The helix, when used in this manner, may be called a "helical beam antenna" and is said to be radiating in the "axial mode."

Although the current distributions of many types of antennas are well known, only a few distributions have been reported for the helical antenna.[2] The current

* Decimal classification: R326.7×R242. Original manuscript received by the Institute, February 3, 1950; revised manuscript received, August 23, 1950.

Work described in this paper was carried out, in part, under a contract between the Wright-Patterson Air Force Base of the Air Materiel Command and the Ohio State University Research Foundation. This is a portion of a doctorate dissertation, entitled, "A study of phase velocity on long cylindrical conductors," presented, Graduate School, Ohio State University, 1949. Presented, 1950 National IRE Convention, New York, N. Y., March 7, 1950. Published as a special report, The Ohio State University Research Foundation, February 28, 1950.

† Formerly, The Ohio State University Research Foundation, Columbus 10, Ohio; now, Aerophysics Laboratory, North American Aviation, Inc., Downey, Calif.

[1] J. D. Kraus, "Helical beam antenna," *Electronics*, vol. 20, pp. 109–111; April, 1947.
[2] J. D. Kraus and J. C. Williamson, "Characteristics of helical antennas radiating in the axial mode," *Jour. Appl. Phys.*, vol. 19, pp. 87–96; January; 1948.
[3] O. J. Glasser and J. D. Kraus, "Measured impedances of helical beam antennas," *Jour. Appl. Phys.*, vol. 19, pp. 193–197; February; 1948.
[4] J. D. Kraus, "Helical beam antennas for wide-band applications," Proc. I.R.E., vol. 36, pp. 1236–1242; October, 1948.
[5] J. D. Kraus, "The helical antenna," Proc. I.R.E., vol. 37, pp. 263–272; March, 1949.

distribution on the helix is complex, and varies in an anomalous manner with changes in frequency. Accordingly, a systematic set of measurements was undertaken in order to observe the current distribution both as a function of distance along the helix and also as a function of the frequency. Examples of these measured distributions and their analysis in terms of traveling waves on the helix are presented in this paper.

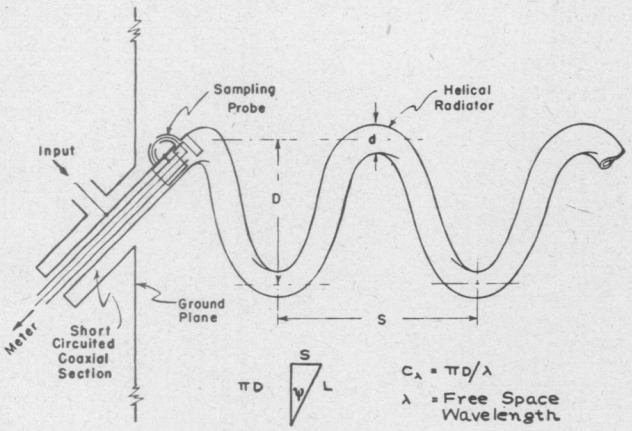

Fig. 1—Sketch of feed and sampling system used in the investigation of the helix.

All of the measurements were made in the uhf range on helices made from copper cylindrical tubing having small outer diameters in terms of a wavelength. Therefore, the assumption is made that the current on the helix is a one-dimensional surface current flowing only in the direction of the conductor axis. This assumption permits the use of the method of feeding and sampling shown in Figs. 1 and 2.[6] The hollow-center conductor

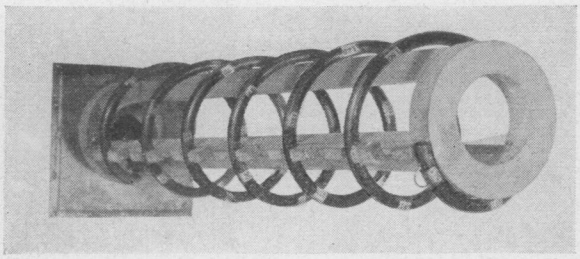

Fig. 2—Six-turn uniform circular helix, pitch angle $\psi = 12.6°$, mean diameter $D = 8.61$ cm.

of a short-circuited coaxial section is extended and wound in the shape of a uniform circular helix. The helix is excited by feeding energy through the side of the coaxial section. The current on the helix is sampled by means of a balanced loop which is positioned in an axial slot in the radiator. The energy sampled by the loop is fed back through the inside of the helix on a coaxial line to the measuring equipment located behind the ground plane.

Since the currents on the helix vary harmonically with time, must satisfy Maxwell's equations, and are assumed to be one-dimensional, it is possible to obtain expressions for the currents by the superposition of one-dimensional traveling waves.

The analysis of a measured current distribution in terms of traveling waves consists of assigning a relative amplitude function and a relative phase velocity to each of the component waves. The analysis becomes difficult for the present case, since there are at least three traveling waves of significant magnitude which, in general, have different phase velocities. For simplicity, the amplitude of the component waves are assumed to be either constant or exponentially attenuated. Therefore, each component wave can be expressed in the form:

$$I = I_0 e^{-\alpha x + j(\omega t \mp \beta x)},$$

where α is the attenuation constant, ω is the angular frequency, and β is the phase constant. The phase velocity of such a wave is usually defined[7] as $v = \omega/\beta$ and is independent of the attenuation constant α. In practical systems, however, the existence of a single traveling wave of the form above is rarely encountered. The current distributions that are usually measured consist of two or more traveling waves, and only the sum total of these currents is measurable.

It is common practice to measure the relative phase and amplitude of the total current as functions of distance and plot these data, choosing a convenient reference point in the system for the co-ordinate, in a manner as shown in Figs. 3 to 5. The relative amplitude curves are labeled $|I(x)|^2$ and the relative phase curves are labeled ϕ. The angle ϕ, essentially a lag angle for waves traveling to the right, is plotted positively for convenience. Since the angular frequency ω is readily determined in any practical measurement, it is only necessary to obtain the wave number β to find the phase velocity. If there were but one wave traveling with a constant velocity in the system under consideration, the $\phi(x)$ curve would be linear with a slope equal to β. The determination of the phase velocity for this case is straightforward. However, where more than one wave is present, the curve is not linear and the determination of β must be made indirectly. That is, an average slope of the ϕ curve, or some other method which uses the distance between successive points which are 360° apart must be employed to obtain the phase velocity.

A generalized phase velocity can be defined for the case where more than one traveling wave is present in the system by letting the slope $d\phi/dx = \beta(x)$ and defining $\hat{v} = -\omega/\beta(x)$, where $\hat{v}$ is called the generalized

[6] This method has been used by a number of investigators; see for example, G. Barzilai, "Experimental determination of the distribution of current and charge along cylindrical antennas," PROC. I.R.E., vol. 37, pp. 825–829; July, 1949. Also, M. Aronoff, "Measured phase velocity and current distribution characteristics of helical antennas radiating in the beam mode," an unpublished thesis for the degree of M.Sc., Ohio State University, 1948.

[7] J. A. Stratton, "Electromagnetic Theory," 1st ed., McGraw-Hill Book Co., Inc., New York, N. Y.; 1941.

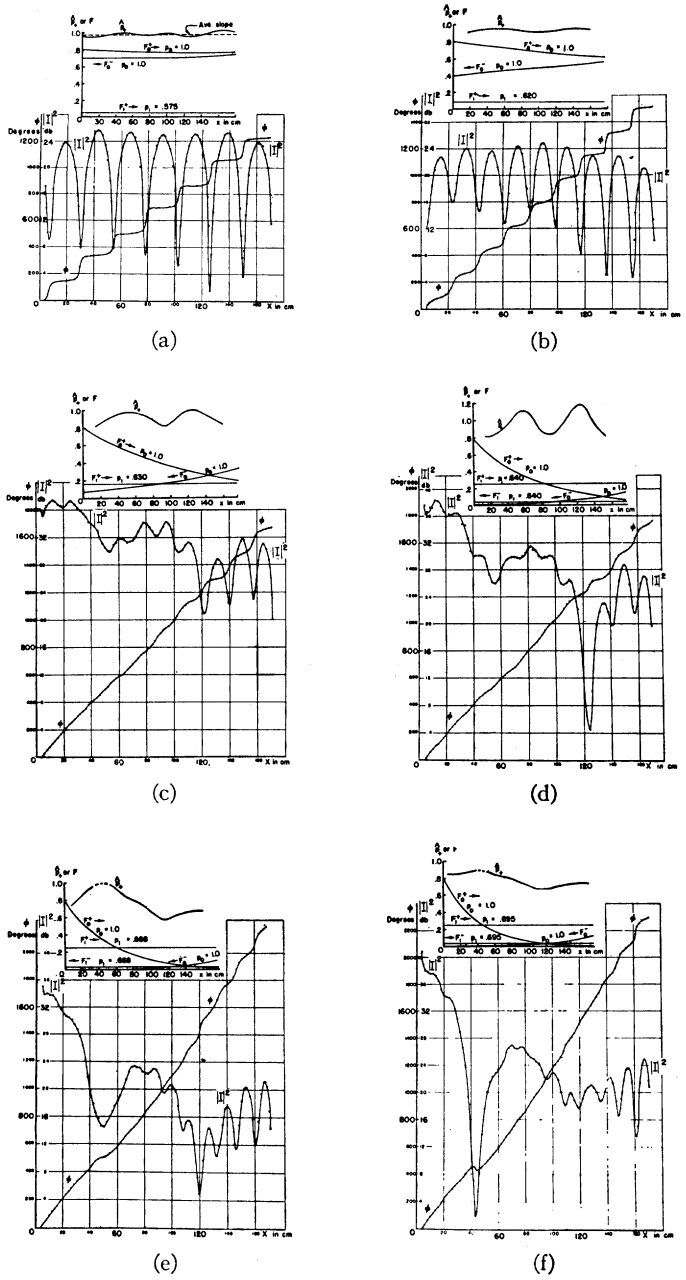

Fig. 3—Measured current distributions on the helix as a function of C_λ, the circumference in wavelengths:
(a) $C_\lambda=0.542$ (b) $C_\lambda=0.665$
(c) $C_\lambda=0.691$ (d) $C_\lambda=0.715$
(e) $C_\lambda=0.774$ (f) $C_\lambda=0.855$.

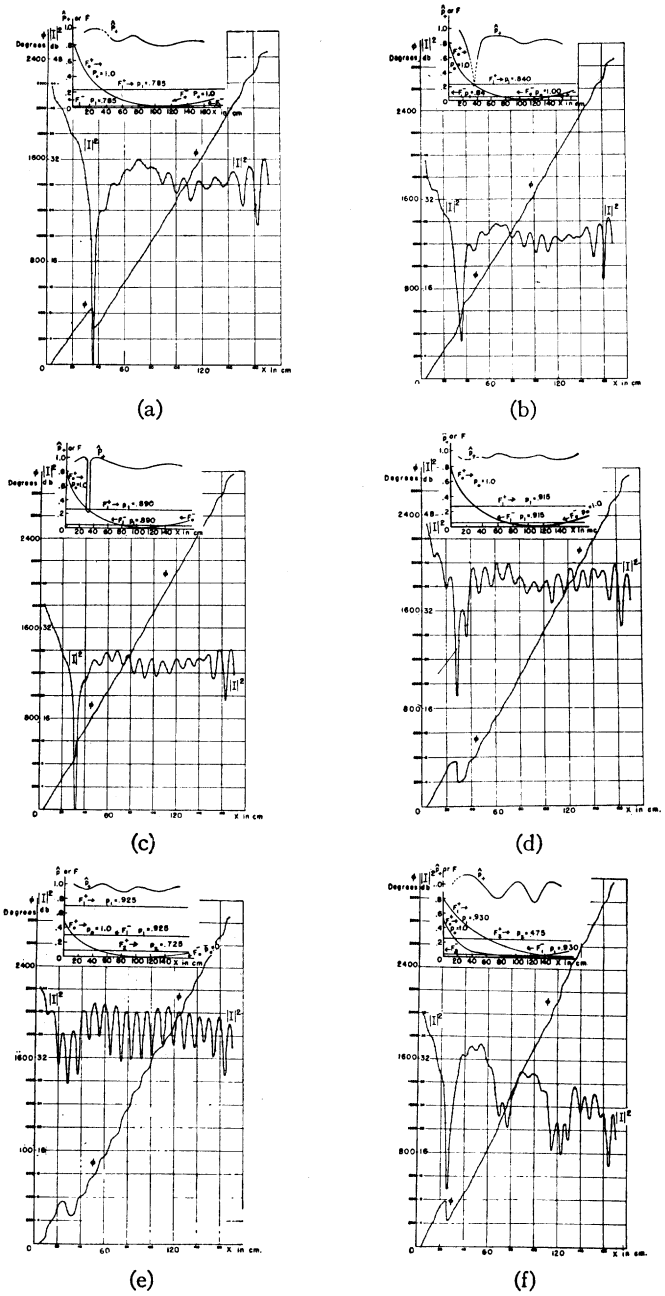

Fig. 4—Measured current distributions on the helix as a function of C_λ, the circumference in wavelengths:
(a) $C_\lambda=1.01$ (b) $C_\lambda=1.09$
(c) $C_\lambda=1.175$ (d) $C_\lambda=1.26$
(e) $C_\lambda=1.36$ (f) $C_\lambda=1.50$.

phase velocity, and the negative sign is necessary because of the convention adopted in plotting ϕ positive for a wave traveling in the positive x direction. Such a generalization leads to many interesting interpretations of phenomena often observed.[8] If ω and $\phi(x)$ are measured or known mathematically, the quantity $\hat{v}$ may be found graphically or calculated directly. Since the phase velocity relative to the velocity of light is usually used to describe the traveling waves in the system, the data are presented in the form $\hat{p}=\hat{v}/c$, where c is the velocity of light and $\hat{p}$ is called the generalized relative phase velocity. Plots of $\hat{p}_+$, the generalized relative phase velocity for those waves traveling in the positive x direction only, may be found in Figs. 3 and 4.

II. Measured Distributions

The antenna investigated (see Fig. 2) is a six-turn helix which has a pitch angle $\Psi=12.6°$, and a mean diameter $D=8.61$ cm. This antenna is mounted on a three-foot-square ground plane which is supported so that the helix is horizontal and about six wavelengths above ground. The current distribution was obtained as a function of distance measured along the slot in the

[8] For a more complete discussion, see J. A. Marsh, "A study of phase velocity on long cylindrical conductors," presented, Graduate School, Ohio State University, 1949. Presented, 1950 National IRE Convention, New York, N. Y., March 7, 1950. Published as a special report, The Ohio State University Research Foundation, February 28, 1950.

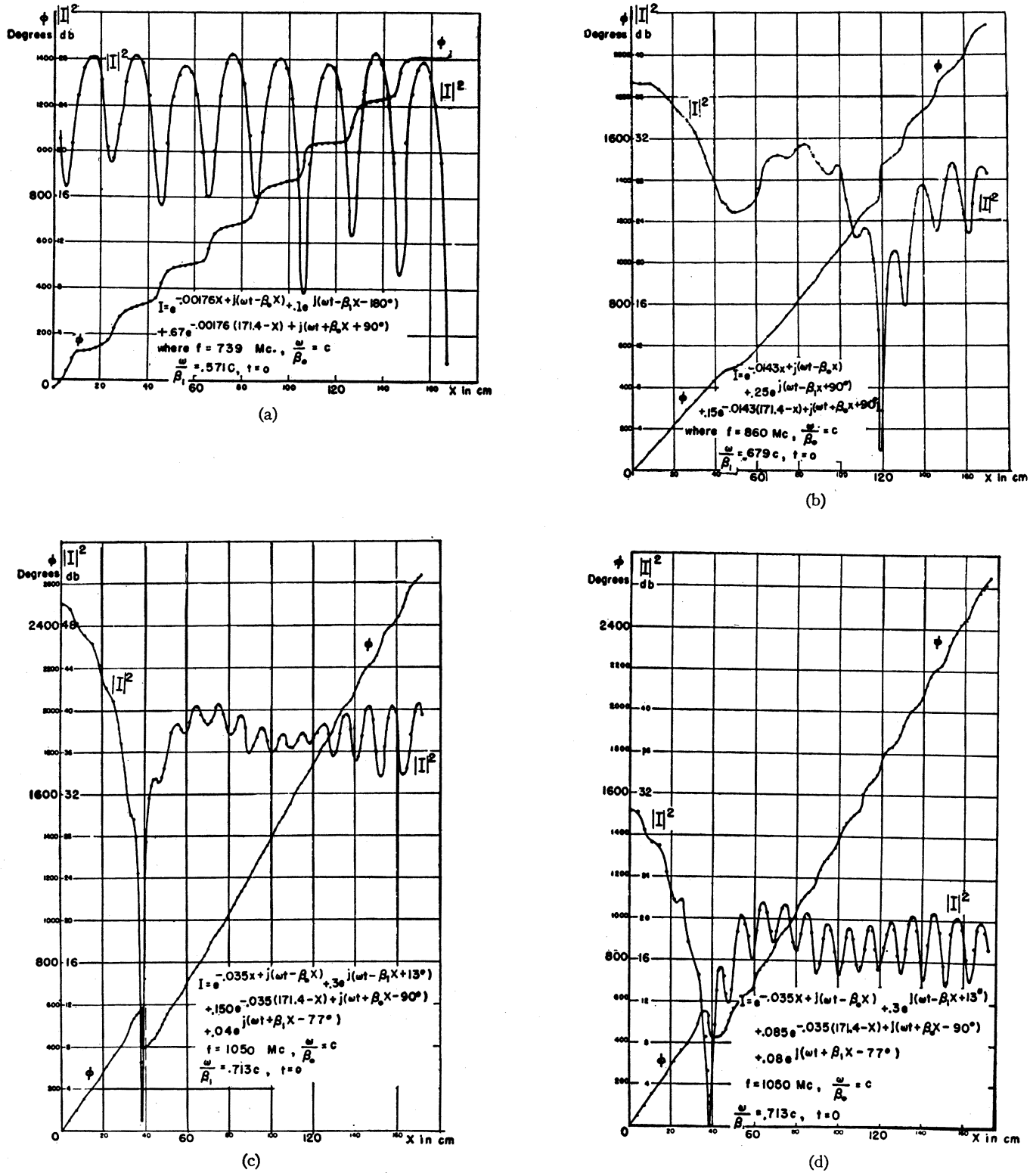

Fig. 5—Calculated current distributions on the helix:
(a) To mode region (compare with Fig. 3(b)).
(b) Transition region from T_0 to T_1 modes (compare with Fig. 3(d)).
(c) T_1 mode region (compare with Fig. 4(a)).
(d) Transition region from T_1 to T_2 modes (Compare with Fig. 4(d) and 4(e)).

hollow tubing using the ground plane as a reference.

The measured current distribution on the helix for the range of frequencies 602 to 1,667 mc may be seen in Figs. 3 and 4. The distributions are labeled in terms of the parameter C_λ, which is defined in Fig. 1 as the circumference in free-space wavelengths of the cylinder with diameter D. The data[9] are arranged in order of increasing C_λ. In each of the distributions shown in

[9] The magnitude of the current I is expressed in decibels relative to an arbitrary reference current I_0 by db $= 10 \log (I^2/I_0^2)$.

Figs. 3 and 4 there is an insert which contains a portion of the analysis made of the data for that distribution. These inserts show an approximate plot of the generalized relative phase velocity, $\hat{p}_+$ for the waves which travel only in the positive x-direction away from the ground plane. The other curves, shown in the inserts, are plots of the amplitude or F functions for the number of one-dimensional traveling waves which may be used to obtain an approximate expression for the current distribution shown. The plus and minus signs are used to show that the associated waves are traveling in the positive or negative x-direction, respectively. It should be stated that these curves are only initial assumptions needed to "fit" the associated distribution. Because of the number of variables involved, the actual task of fitting any one of these curves closely is tremendous. Thus, no attempt was made to "fit" a particular distribution exactly. Four distributions (see Fig. 5) were calculated to show how distributions in four different regions of C_λ could be obtained.

III. Analysis

In the analysis of the data shown in Figs. 3 and 4, it is found that the current distributions can be interpreted in terms of traveling waves associated with three different modes of transmission on the helix. These modes[5] are distinguished by means of the symbols T_0, T_1, and T_2. The T_0 mode of transmission on the helix is found to predominate when $C_\lambda < 0.675$. This is the mode of transmission which is encountered in the traveling wave tube. The T_1 mode of transmission predominates when C_λ lies in the region from 0.80 to 1.30. Since the T_1 mode of transmission on the helix makes possible the axial or beam mode of radiation, it is the center of interest in this investigation. The T_2 mode of propagation exists when $C_\lambda > 1.25$. The presence of energy in this mode is first detected at the upper frequency limit of the helical beam antenna. The subscripts 0, 1, and 2 are used in the inserts of Figs. 3 and 4 to connect the relative amplitude functions and phase velocities of the traveling waves with these transmission modes.

A. The T_0 Mode Distribution

The current distribution shown in Fig. 3(a) is a typical example of the distributions found in the range of frequencies where C_λ varies from 0.348 to 0.600. Traveling waves of current, which may be associated with the T_0 mode of transmission, predominate in this range of frequencies. The amplitudes of the T_0 traveling waves encounter only a slight attenuation and the waves are assumed to travel with the velocity of light. This results in an amplitude characteristic which has a large standing-wave ratio and a phase characteristic which is nearly a step function.

The presence of T_1 mode currents may be detected in the current distributions when $C_\lambda = 0.542$ and 0.665 (see Fig. 3(a), (b)) by observing the undulating nature of the $\hat{p}_+$ curves in the inserts. However, the relative importance of the T_1 mode currents in these two distributions is very slight.

A calculated T_0-mode-region current distribution is presented in Fig. 5(a). This distribution is a first attempt to approximate the measured current distribution shown in Fig. 3(b), when $C_\lambda = 0.665$. Although it is obvious from a comparison of the two distributions that refinements on the first attempt could be made, it is felt that the calculated distribution shows clearly that, by minor manipulations of the available parameters of the three traveling waves, one could obtain calculated and measured distributions which agree within experimental accuracy. The assumed current expression consists of two T_0-mode traveling waves which travel with the velocity of light in opposite directions and have a slight exponential amplitude attenuation. The third, T_1 mode, wave is assumed to be constant in amplitude and to travel with a relative velocity $p_1 = 0.571$.

B. The Transition Region from the T_0 to the T_1 Mode

The transition region from the range of frequencies where the T_0 mode predominates to the range of frequencies where the T_1 mode predominates, occurs in the range $C_\lambda = 0.675$ to $C_\lambda = 0.800$. A study of the measured current distributions in Fig. 3 shows how this transition occurs. A calculated current distribution for this region of transition is given in Fig. 5(b) and is seen to approximate the measured distribution when $C_\lambda = 0.715$.

A comparison of the expressions used to obtain Figs. 5(a) and 5(b) shows that the amplitude of the two waves associated with the T_0 mode become more sharply attenuated as C_λ is increased. This results in less total energy reaching the open end of the helix, and therefore, less energy reflected to create standing waves. The traveling waves associated with the T_1 mode begin to take on more and more importance in this region of transition, not only because of the increased attenuation encountered by the T_0 waves, but also because of the increase in the relative value of the constant amplitude of the T_1 waves compared to the amplitude of the T_0 waves at $x = 0$.

C. The T_1 Mode Distribution

The T_1 or beam mode of radiation from the circular helix may be said to occur in the range of frequencies where C_λ takes on the values 0.8 to 1.3. Figs. 3 and 4 show measured current distributions obtained in this region. A study of these data reveals that although the attenuated waves associated with the T_0 mode are always in evidence they attenuate rapidly so that the T_1 waves predominate a few turns from the feed point. Most of the energy which reaches the open end of the helix is reflected in the form of a T_0 wave, but this also attenuates rapidly leaving only the F_1^+ wave to pre-

dominate over most of the helix. This results in only a small reflected wave reaching the feed end of the helix and accounts for the relatively constant input impedance as a function of frequency. Fig. 5(c) shows a calculated current distribution which should be compared with the measured distributions when $C_\lambda = 1.01$ (see Fig. 4(a)).

The amplitude characteristic of the current distribution in the T_1 mode region can best be explained by observing a trend which may be seen in Figs. 3 and 4. When $C_\lambda = 0.691$ (see Fig. 3(c)), there are two minima which occur at $x = 53$ and 123 cm. As C_λ takes on higher values, the minimum, which occurs in the vicinity of $x = 120$ cm, first becomes more pronounced and then disappears when C_λ has values greater than 1.0. The minimum in the vicinity of $x = 50$ cm goes through the same variation and happens to be very pronounced in the distributions which occur in the range of frequencies where the T_1 mode is said to predominate. Similar minima occur again in the distributions when C_λ is greater than 1.4.

These minima can be interpreted as the points where the F_0^+ and F_1^+ waves interfere since the two waves are traveling in the same direction with different phase velocities. The depths of the minima are controlled by the relative magnitudes of the two waves when they are in phase opposition. The increase in attenuation which the T_0 mode currents encounter, as C_λ is increased, causes the minima first to become more pronounced as the initially larger F_0^+ wave attenuates to a value almost equal to the smaller, but constant F_1^+ wave. Then as the attenuation of the F_0^+ wave becomes large, the magnitude of this wave becomes so small compared to the F_1^+ wave at a point of interference that the minima cannot be observed.

The position of these minima, created by the outward traveling waves, is sometimes obscured and other times accentuated by the presence of reflected energy from the open end of the helix. The reflected waves also propagate in at least two modes. When C_λ has values between 1.0 and 1.3, the SWR created by the reflected wave varies in a beatlike fashion. The points of small SWR can be interpreted as points of interference between the F_0^- and F_1^- waves.

Plots are presented in Fig. 6 of the component traveling waves which combine to produce the distribution shown in Fig. 5(c). These plots show how the F_0^+ and F_1^+ waves add to give the total outward traveling current distribution as well as the manner in which the reflected F_0^- and F_1^- waves combine to give the total reflected current distribution. Fig. 6 reveals how the pronounced minimum in the amplitude characteristic is obtained by the interference of the F_0^+ and F_1^+ waves. In addition, one observes in the absence of any reflected waves that there is a very rapid phase advance in the vicinity of the point of maximum interference ($x \cong 1.25\lambda_0$). However, since the outward traveling currents are at such a low level at this point, the reflected energy predominates and causes a reversal of the direction of energy flow over this short segment of the helix. Therefore, the total phase characteristic encounters a dip. It is observed in Figs. 3 and 4 that this effect is encountered many times in measurements; however, occasionally the reflected energy is not large enough to create the phase reversal, and the inherent phase jump is measured. (See Figs. 4(b), 4(c)).

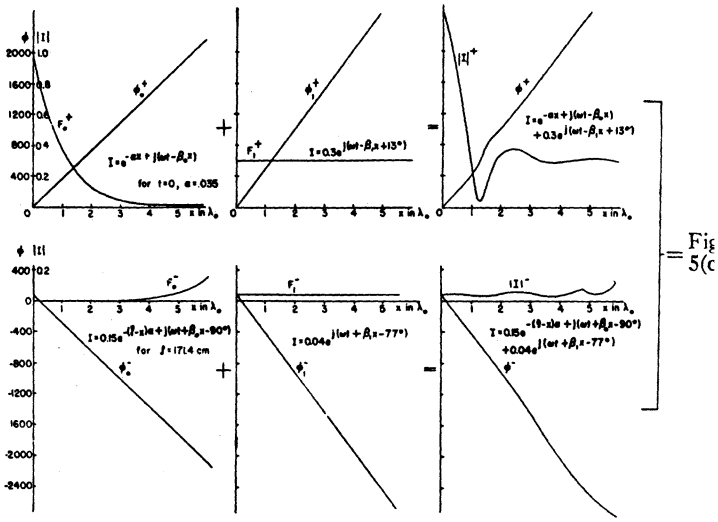

Fig. 6—Component traveling waves and the manner in which they add to produce a T_1 mode current distribution. (a) Outward traveling waves. (b) Reflected traveling waves.

D. The Transition from the T_1 to the T_2 Mode

The effect of the T_2 mode currents upon the total current distribution may be observed in Fig. 4(e), 4(f), when $C_\lambda = 1.36$ and 1.50. The transition phenomena observed in this range of values for C_λ is quite similar to those observed in the transition region between the T_0 and T_1 modes discussed above; therefore, only a few general observations will be made.

The presence of a T_2 mode on the helix has been detected by earlier investigators.[5,10] However, the radiation pattern of the helix in the range of frequencies where the presence of this mode has been detected[10] has broken up into a large number of lobes. Therefore, the investigation of the helix in this range of frequencies has not been stressed.

A calculated current distribution for the transition region from the T_1 to T_2 modes is illustrated in Fig. 5(d), and should be compared with the measured distributions shown in Figs. 4(d), 4(e), when $C_\lambda = 1.26$ and 1.36.

In the insert of Fig. 4(f), one will observe that the F_1^+ wave has an exponential attenuation. When C_λ is made larger than 1.4, the T_1 mode also develops an

[10] C. K. Bagby, Jr., "A theoretical investigation of electromagnetic wave propagation on the helical beam antenna," an unpublished thesis for the degree M.Sc., The Ohio State University, 1948.

exponential attenuation similar to that of the T_0 mode discussed above.

IV. Phase Velocity

It is apparent from the above analysis that there are always two modes of propagation present on the helix in the range of frequencies where a detailed investigation has been made. This means that there is no single phase velocity associated with the helix, except in certain regions of the helix at certain frequencies. At any given frequency there are always traveling waves which can be associated with two or more different modes, each of which has its own characteristic phase velocity. In analyzing the measured current distributions of Figs. 3 and 4 it is possible to distinguish the different modes present and their relative phase velocities. The results of this analysis may be seen in Fig. 7, where the p versus C_λ curves for the individual modes are given.

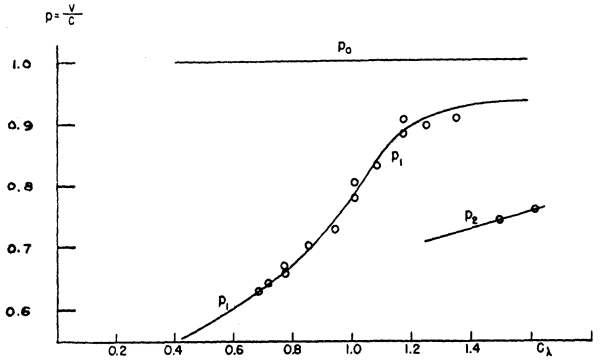

Fig. 7—p versus C_λ curves for the T_0, T_1, and T_2 modes on the helix.

It has been shown by Pierce,[11] and by Chu and Jackson,[12] that propagation along the helix in the T_0 mode has a characteristic phase velocity greater than the velocity of light. This velocity decreases as C_λ increases and approaches closely to the velocity of light when $C_\lambda > 0.7$. Therefore, the relative phase velocity p_0 of the T_0 mode is assumed to be 1.0 at all larger values of C_λ. The maximum error introduced by this assumption occurs for small values of C_λ, and amounts to about 2 per cent when $C_\lambda = 0.7$.

In Fig. 7, one observes that p_1 and p_2 are functions of frequency and are always less than 1.0 in the range of the measurements. The quantities p_1 and p_2 are the phase velocities of the traveling waves associated with the T_1 and T_2 modes, respectively, relative to the velocity of light. The relative phase velocities assigned to each of the traveling waves in the inserts of Figs. 3 and 4 were obtained from Fig. 7. The information available in the inserts of Figs. 3 and 4, therefore, should enable one to calculate, to a good approximation, the far field-radiation pattern of the helix. The radiation pattern of the helix operating in the beam mode has been calculated by Kraus,[2,5] assuming that the current distribution is essentially a single unattenuated outward-traveling wave. This is a satisfactory approximation for a long helix. Kraus uses a phase velocity measured in the central portion of a seven-turn helix and good agreement is obtained between calculated and measured patterns.

The inserts of Figs. 3 and 4 show that the current distribution on the helix when operating in the T_1 mode is essentially the F_1^+ wave. Therefore, in the T_1 mode the p_1 versus C_λ curve should agree fairly closely with a measured p versus C_λ curve obtained by Kraus.[13] The two curves are plotted in Fig. 8 for comparison. The maximum directivity line also shown in Fig. 8 was obtained from an expression derived by Kraus.[5] This expression

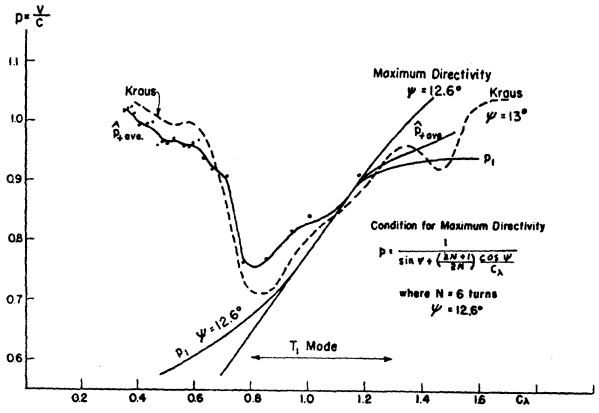

Fig. 8—p curves for the uniform circular helix.

gives the value p should have for the radiation from an array of helical turns, considered as point sources, to add up along the axis of the helix in such a manner as to produce maximum directivity in the axial direction. In Fig. 8, it is observed that the p_1 curve, the maximum directivity curve, and Kraus' curve are all in close agreement within the region of the T_1 mode.

Since the task of calculating the radiation pattern for the helix is laborious at best, it would be desirable to reduce to at least two the number of traveling waves considered, even outside the region of the T_1 mode. In the T_1 mode, the F_1^+ wave alone may be used to calculate the patterns as has been done by Kraus. However, at both ends of the T_1 mode region and beyond, the traveling waves associated with the other modes cannot be neglected.

To facilitate calculations, it is suggested that all of the energy which flows in the positive x direction be considered as one traveling wave, which has a phase velocity that is weighted in terms of the relative magnitudes of the component traveling waves which it is approximating. The energy which flows in the negative x direction can be treated in the same manner. The

[11] J. R. Pierce, "Theory of the beam-type traveling wave tube," Proc. I.R.E., vol. 35, pp. 111–123; February, 1947.

[12] L. J. Chu and D. Jackson, "Field theory of traveling wave tubes," Proc. I.R.E., vol. 36, pp. 853–863; July, 1948.

[13] J. D. Kraus, "Antennas," McGraw-Hill Book Co., Inc., New York N. Y., in press; see Figs. 7–19.

generalized phase velocity, defined above, is such a weighted phase velocity. In the inserts of Figs. 3 and 4, one will notice curves which are labeled $\hat{p}_+$. These curves are plots of the generalized phase velocity for the energy traveling in the positive x direction only. These curves were obtained from calculations made on the associated measured current distribution. In drawing the $\hat{p}_+$ curves, the regions where the associated ϕ versus x curve dips were omitted for two reasons: first, the peculiar behavior in the region of the phase dips is almost always created by the reflected wave and, therefore, should not be allowed to affect $\hat{p}_+$; second, the current in this region is always down in amplitude from the maximum by a factor of 20 db and the effect this small segment of the helix can have on the over-all radiation must be negligible.

The shape and trends shown by these $\hat{p}_+$ curves are interesting. Each of the four regions discussed have $\hat{p}_+$ curves which may be considered characteristic of that region. In the region of the T_0 mode, the $\hat{p}_+$ curve is fairly constant and has a value between 0.95 and 1.0. The $\hat{p}_+$ curve has an oscillatory nature in the regions of transition from one mode to another. The oscillations are similar to those observed when two waves are traveling at different velocities in the same direction. The center of oscillation, of course, shifts down as the T_1 mode currents tend to predominate. The $\hat{p}_+$ curves in the T_1 mode region are characteristically high for low values of x where the T_0 mode currents are still large. As the value of x increases, the $\hat{p}_+$ curve settles down to the value p_1 for most of the remaining length of the helix. The $\hat{p}_+$ curves are often more sensitive indications of the presence of other modes than are the amplitude and phase curves themselves.

Each of the generalized $\hat{p}_+$ curves was integrated graphically and the average value plotted in Fig. 8. The curve drawn through these points is labeled $\hat{p}_{+\text{ave}}$. The values of p, obtained from this curve, can be used as a weighted phase velocity for a single traveling wave approximation of the energy traveling in the positive x direction. It is observed that this curve follows roughly Kraus' curve in Fig. 8. Differences between these two curves should be expected since the $\hat{p}_{+\text{ave}}$ curve is an average taken over the entire helix, whereas Kraus' curve was measured in the central region of a seven-turn helix.

V. Charge and Current on a Long Helix

The above analysis has been made almost entirely on the basis of data obtained from the helix shown in Fig. 2. As a check on this analysis, a second helix was constructed similar to the antenna of Fig. 2 but with 3.75 additional turns.

From the analysis made on the shorter helix, one should be able to predict the effect of extending the helix in length. For example, when $C_\lambda = 0.774$ (see Fig. 3(e)), the total current distribution is relatively free of any reflected energy when $x < 80$ cm. Extending the length of the helix at this frequency, therefore, should not alter the current distribution appreciably in the region $x < 80$ cm. However, by making the helix longer one would expect the amplitude curve in the vicinity of $80 \leqq x \leqq 160$ cm to be smoothed out since the attenuated reflections would occur at some point beyond $x = 172$ cm.

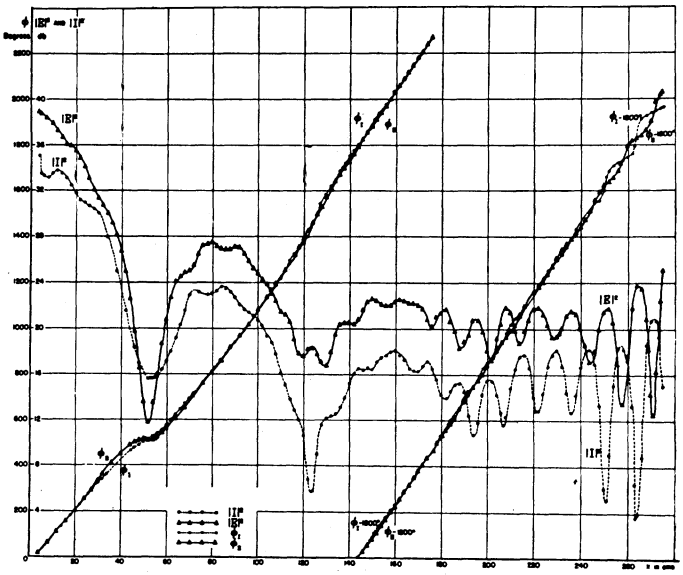

Fig. 9—Measured current and charge distribution on a 9.75-turn helix, pitch angle $\psi = 12.6°$, mean diameter $D = 8.61$ cm for $C_\lambda = 0.774$.

The current distribution shown in Fig. 9 was measured on the long helix, 9.75 turns, for $C_\lambda = 0.774$. Comparing Fig. 9 with Fig. 3(e) for the six-turn helix at the same value of C_λ, one finds that all of the predictions are fulfilled.

As a further check on the analysis, a charge or E field measurement as a function of distance along the long helix was made and plotted in Fig. 9. Comparing the E and H field measurements shown in Fig. 9, one observes that for low values of x, where the outward traveling waves predominate, the E and H fields are in phase and have the same general shape. However, as x takes on larger values, the effect of the reflected energy causes the E and H fields to approach a relative phase quadrature. That is, the two phase characteristics take on an interlaced appearance, a maximum E field amplitude being found where a minimum H field is observed, and vice versa.

VI. Acknowledgment

The advice and encouragement of J. D. Kraus, and the assistance received from the staff of the Ohio State University Research Foundation Antenna Laboratory, are gratefully acknowledged.